Journal of Sound and Vibration (2002) **252**(1), 155–167
doi:10.1006/jsvi.2001.4038 available online at http://www.idealibrary.com on IDEAL®

TRANSVERSE VIBRATION OF ELASTIC–VISCOELASTIC–ELASTIC SANDWICH BEAMS: COMPRESSION—EXPERIMENTAL AND ANALYTICAL STUDY

C. L. Sisemore† and C. M. Darvennes

Department of Mechanical Engineering, Tennessee Technological University, P.O. Box 5014, Cookeville, TN 38505, U.S.A.

Experimental and analytical results are presented from an investigation into the compressional vibration of an elastic–viscoelastic–elastic three-layer sandwich beam. Most analytical models make the fundamental assumption that shear deformation in the viscoelastic core yields the largest damping and compressional deformation is negligible. Experimental results from a cantilever beam with a constrained layer viscoelastic damping treatment driven with a sinusoidal input are given which show compressional deformation over a relatively wide driving frequency range. A new analytical model for compressional damping is presented and compared with experimental results, with the Mead and Markus shear damping model, and with the Douglas and Yang compressional damping model. These results indicate that the proposed compressional model is a better predictor of resonance frequencies for the cantilever beams tested and that all models show deficiencies in predicting damping

1. INTRODUCTION

The use of sandwich beams with embedded viscoelastic damping material has become relatively common for vibration and noise control. The three-layer damped beam arrangement consists of a layer of high-damping viscoelastic material bonded to a machine or structural component with an additional layer of elastic material bonded to the outer surface of the viscoelastic material, thus creating a three-layer sandwichtype structure with a viscoelastic damping core. The effect of the outer elastic layer, the constraining layer, is to increase the deformation in the viscoelastic core, thus resulting in higher energy dissipation in the viscoelastic material. There are two primary methods for dissipating energy in the viscoelastic core of a constrained layer damping treatment—shear deformation and compressional deformation. Shear deformation results when the constraining layer and the base structure move parallel to each other, acting to shear the viscoelastic core. Compressional or extensional deformation results when the constraining layer and the base structure move perpendicular to each other, acting to compress or stretch the viscoelastic material.

The vast majority of the research in this area has focused on the shear method of dissipating energy. In fact, the vast majority of researchers in this area make the

†Current address: Naval Surface Warfare Center; 17320 Dahlgren Rd; Dahlren, VA 22448, U.S.A.

0022-460X/02/$35.00

assumption that transverse displacements of all points on a cross-section are equal, and hence, compressional damping does not occur or is negligible. The earliest of these are papers by Kerwin and DiTaranto [1, 2] which focused on mathematical modelling of long, simply supported beams with soft viscoelastic cores and thin, stiff constraining layers. In a series of later papers, Mead and Markus [3–5], developed a sixth order differential equation of motion in terms of the transverse displacement of the beam for arbitrary boundary conditions. The analytical work presented by Mead and Markus makes the fundamental assumption that shearing of the viscoelastic core is the only mechanism for energy dissipation and that compressional damping does not occur. Mead and Markus work has become the generally accepted method of modelling and describing damped three-layer beams and plates.

Later, Douglas and Yang [6, 7] showed experimentally that transverse compressional damping can become the dominant damping method in narrow frequency bands under certain conditions. In addition, Douglas and Yang presented a mathematical model for compressional damping in three-layer beams. Sylwan [8] developed a model to combine shear and compressional damping effects in layered beams with thin damping cores showing increased losses over a wider frequency range than could be predicted by either shear damping or compressional damping alone. More recently, Lee and Kim [9] presented mathematical results suggesting that neglecting compressional damping in the analysis of beams and plates with constrained viscoelastic damping layers would only give acceptable results for very thin viscoelastic layers.

Finally, Sisemore *et al.* [10, 11] presented experimental results from a cantilever beam under impact loading and from an operating four-bar mechanism with a damped coupler link that show compressional damping in the viscoelastic core.

It is the aim of this research to show the extent to which compressional damping can exist in the viscoelastic core and to offer a new analytical model for calculating the frequency response of damped beams subject to compressional damping only. This model is compared with experimental results to determine its validity.

2. EXPERIMENTAL EVALUATION

The first experiment was designed to measure the response of a cantilever beam with a constrained layer of viscoelastic damping material to a steady-state sinusoidal input. The experimental set-up, shown in Figure 1, used two MTI Fotonic fiber optic displacement sensors to measure the free end displacement of the base beam and the constraining layer. An MB Dynamics Modal 50 vibration exciter drove the beam via a stinger that was threaded into the free end of the base beam. The vibration exciter was suspended above the cantilever beam by attaching the exciter to a steel support frame using wire rope. The same rigid base was used to support the vibration exciter support frame and the test fixture. A series of steady-state sinusoidal inputs were provided to the vibration exciter from a programmable signal generator. The displacements of the beam and constraining layer were measured using a computer data acquisition system. With this arrangement, it was possible to directly measure any compressional vibration in the viscoelastic core. The two fiber optic displacement sensors were mounted such that one sensor measured the displacement of the constraining layer at a given point while the second sensor measured the displacement at the corresponding point on the base beam. A direct comparison of the two displacements determines the amount of relative motion between the constraining layer and the base beam.

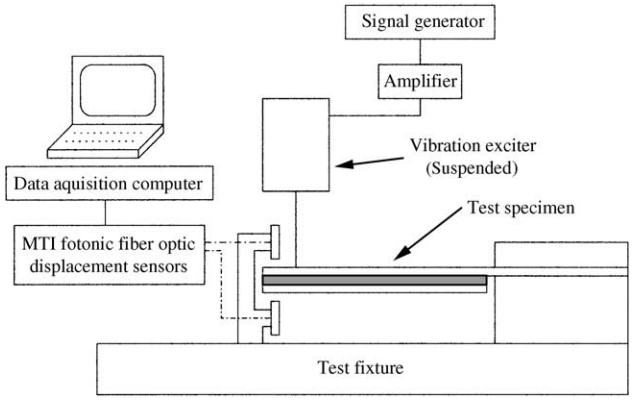

Figure 1. Experimental set-up.

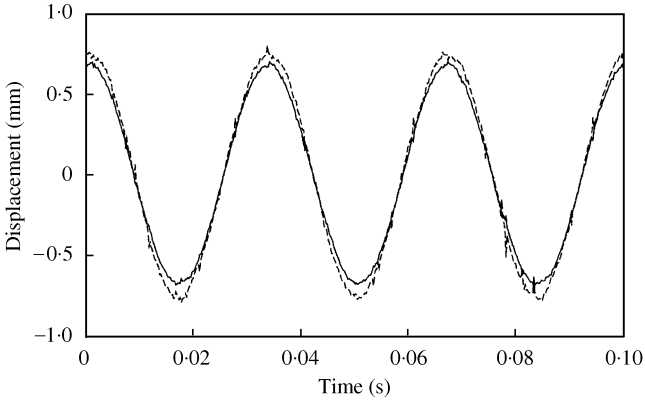

Figure 2. Steady-state tip response to a 30 Hz sinusoidal input (——, base beam; - - - - -, constraining layer).

The beam for this experiment was 6·35 mm thick, the viscoelastic layer was 3·05 mm thick, and the constraining layer was 3·18 mm thick. All three layers were 25·4 mm wide. The base beam was 314 mm long and the viscoelastic and constraining layers were 305 mm long, with the difference providing a small relief at the clamped end to prevent interference between the constraining layer and the test clamp. The test beam and its constraining layer were constructed of aluminum with the following standard properties: modulus of elasticity $E = 71$ GPa, shear modulus $G = 26{\cdot}2$ GPa, and density $\rho = 2710\,\text{kg/m}^3$. The viscoelastic layer was made of EAR-C1002 viscoelastic material bonded to the aluminum layers with Bostik 7132/Boscodur #4 two-part epoxy.

The beam was driven with a sinusoidal input at over 40 different frequencies ranging from 25 up to 400 Hz. At each frequency step, the system was allowed sufficient time to reach steady-state conditions before taking data. Figure 2 shows the tip response of the cantilever beam to a 30 Hz steady-state sinusoidal input and is typical of the response measured over the frequency range tested. The responses of the beam and constraining layer were measured and for comparison, the relative amplitude difference between the beam and constraining layer was calculated by

$$D_R = (D_B - D_L)/D_B, \tag{1}$$

where D_R is the relative displacement, D_B is the steady state displacement amplitude of the base beam, and D_L is the steady state displacement amplitude of the constraining layer.

Figure 3 shows the relative displacements calculated over the tested frequency range as well as the actual amplitudes measured for comparison. The results indicate that for this test configuration, the vibration amplitude of the constraining layer is greater than the amplitude of the base beam in all cases. On average, the relative difference between the base and constraining layer was around 13%. Most of the values fell within a narrow range from 10 to 17% relative displacement with a few outlying values reaching as high as 49% and as low as 0·5%.

These results show a continuous trend of compressional vibration in the viscoelastic core over a relatively wide range of frequencies. The general assumption in the literature is that there is no compressional vibration, or if there is any, it occurs over a very narrow frequency bandwidth known as the compressional delamination frequency [6]. In contrast, for the beam tested here, the compressional delamination frequency bandwidth ranges from around 800 up to 2100 Hz, based on the excitation frequency. The reason for the wide range of compressional delamination frequencies is that the viscoelastic material properties change with driving frequency. Thus, at driving frequencies around 25 Hz, the delamination frequency is near 800 Hz and, as the driving frequency increases to 400 Hz, the delamination frequency increases to around 2100 Hz. Since the delamination frequencies are well outside the range of driving frequencies in this experiment and yet compressional vibration does occur, we conclude that compressional damping occurs to some extent at any excitation frequency. It is, however, the dominant damping mechanism at the compressional delamination frequency [6].

3. ANALYTICAL MODEL FOR COMPRESSIONAL DAMPING

Based on the results obtained from the steady-state sinusoidal input experiment, a new analytical model was developed. It assumes that only compressional damping occurs. This model can then be combined with a shear damping model to estimate the behavior of real systems. The equations of motion for a damped three-layer composite beam can be easily derived by use of the extended Hamilton's principle which can be expressed in the form

$$\int_{t_1}^{t_2} (\Delta T - \Delta V)\, \mathrm{d}t = 0, \tag{2}$$

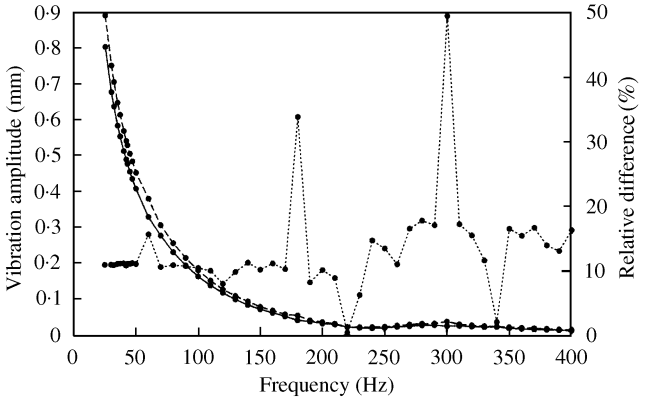

Figure 3. Comparison of beam and constraining layer vibration amplitudes (——, base beam; - - - - -, constraining layer; ····, percent difference).

where ΔT and ΔV are the variations in the kinetic and potential energies of the system, respectively.

From the beam shown in Figure 4, it can be easily seen that the kinetic energy from transverse vibration in the z direction is given by

$$T(x,t) = \frac{1}{2}\int_0^L m_1\left(\frac{\partial w_1}{\partial t}\right)^2 \mathrm{d}x + \frac{1}{2}\int_0^L m_2\left(\frac{\partial w_2}{\partial t}\right)^2 \mathrm{d}x + \frac{1}{2}\int_0^L m_3\left(\frac{\partial w_3}{\partial t}\right)^2 \mathrm{d}x, \tag{3}$$

where $w_i = w_i(x,t)$ and m_i are the transverse displacement and the mass per unit length of the ith layer of the composite beam, respectively. In this development, the base beam is denoted by the subscript 1, the viscoelastic core by subscript 2, and the constraining layer by subscript 3. Several previous researchers have assumed that the mass of the viscoelastic material is negligible, however, this is not necessarily true, especially in systems constructed with light-weight beams and constraining layers, and relatively thick viscoelastic cores. In addition, it is convenient to define the displacements of the viscoelastic core in terms of the displacements of the base beam and constraining layer. Since the viscoelastic core is relatively soft with respect to the two elastic layers, its displacement can be assumed to be completely defined as a linear function of the displacements of the two elastic layers. Thus, the mid-plane displacement of the viscoelastic core is simply the average displacement of the base and constraining layers:

$$w_2 = \tfrac{1}{2}w_1 + \tfrac{1}{2}w_3. \tag{4}$$

The potential energy terms in the extended Hamilton's principle formulation are the sum of the effects of the potential energy from bending of the three-layer beam and from compression or stretching of the viscoelastic core. Assuming Euler–Bernoulli beam theory, we write the potential energy from bending as

$$V(x,t) = \frac{1}{2}\int_0^L E_1 I_1\left(\frac{\partial^2 w_1}{\partial x^2}\right)^2 \mathrm{d}x + \frac{1}{2}\int_0^L E_3 I_3\left(\frac{\partial^2 w_3}{\partial x^2}\right)^2 \mathrm{d}x, \tag{5}$$

where $E_i I_i$ is the bending stiffness or flexural rigidity of the ith layer of the beam. The potential energy from bending of the viscoelastic core is neglected due to the softness of the viscoelastic core in comparison with the elastic layers.

Now, it is assumed that the viscoelastic core is sufficiently soft that it can be modelled as a complex compression spring. The potential energy from compression of the viscoelastic core would then be given by

$$V(x,t) = \frac{1}{2}\int_0^L k^*(w_1 - w_3)^2 \,\mathrm{d}x, \tag{6}$$

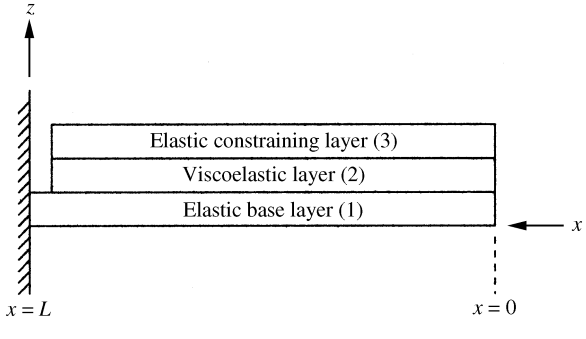

Figure 4. Geometry and co-ordinate system for the three-layer beam.

where k^* is the complex spring constant per unit length for a complex axial compression spring. It is given by $E_v^* b/t_v$, where E_v^* is the complex elastic modulus of the viscoelastic material, b is the beam width, and t_v is the viscoelastic core thickness.

Combining equations (3)–(6), we write the kinetic and potential energy equations in terms of the displacements of the base and constraining layers only. Next, we perform the operations involved in the extended Hamilton's principle. The variation in the kinetic energy gives

$$\delta T = \int_0^L m_1 \frac{\partial w_1}{\partial t}\frac{\partial}{\partial t}\delta w_1 \,\mathrm{d}x + \frac{1}{4}\int_0^L m_2 \frac{\partial w_1}{\partial t}\frac{\partial}{\partial t}\delta w_1 \,\mathrm{d}x + \frac{1}{4}\int_0^L m_2 \frac{\partial}{\partial t}\delta w_1 \frac{\partial w_3}{\partial t}\mathrm{d}x + \frac{1}{4}\int_0^L m_2 \frac{\partial w_1}{\partial t}\frac{\partial}{\partial t}\delta w_3 \,\mathrm{d}x + \frac{1}{4}\int_0^L m_2 \frac{\partial w_3}{\partial t}\frac{\partial}{\partial t}\delta w_3 \,\mathrm{d}x + \int_0^L m_3 \frac{\partial w_3}{\partial t}\frac{\partial}{\partial t}\delta w_3 \,\mathrm{d}x, \quad (7)$$

assuming that the order of the variations and differentiations with respect to time are interchangeable. Similarly, the variation in the potential energy is given by

$$\delta V = \int_0^L E_1 I_1 \frac{\partial^2 w_1}{\partial x^2}\frac{\partial^2}{\partial x^2}\delta w_1 \,\mathrm{d}x + \int_0^L E_3 I_3 \frac{\partial^2 w_3}{\partial x^2}\frac{\partial^2}{\partial x^2}\delta w_3 \,\mathrm{d}x + k^* \int_0^L w_1 \delta w_1 \,\mathrm{d}x - k^* \int_0^L \delta w_1 w_3 \,\mathrm{d}x - k * \int_0^L w_1 \delta w_3 \,\mathrm{d}x + k^* \int_0^L w_3 \delta w_3 \,\mathrm{d}x. \quad (8)$$

Substituting equations (7) and (8) into equation (2), integrating by parts and grouping like terms gives

$$-\int_{t_1}^{t_2} \left\{ \left[-\frac{\partial}{\partial x}\left(E_1 I_1 \frac{\partial^2 w_1}{\partial x^2}\right)\right]\delta w_1\Big|_0^L + \left[-\frac{\partial}{\partial x}\left(E_3 I_3 \frac{\partial^2 w_3}{\partial x^2}\right)\right]\delta w_3\Big|_0^L + E_1 I_1 \frac{\partial^2 w_1}{\partial x^2}\delta\frac{\partial w_1}{\partial x}\Big|_0^L + E_3 I_3 \frac{\partial^2 w_3}{\partial x^2}\delta\frac{\partial w_3}{\partial x}\Big|_0^L + \int_0^L \left[m_1 \frac{\partial^2 w_1}{\partial t^2} + \frac{1}{4} m_2 \left(\frac{\partial^2 w_1}{\partial t^2} + \frac{\partial^2 w_3}{\partial t^2}\right) + \frac{\partial^2}{\partial x^2}\left(E_1 I_1 \frac{\partial^2 w_1}{\partial x^2}\right) + k^* w_1 - k^* w_3 \right]\delta w_1 \,\mathrm{d}x + \int_0^L \left[\frac{1}{4} m_2 \left(\frac{\partial^2 w_1}{\partial t^2} + \frac{\partial^2 w_3}{\partial t^2}\right) + m_3 \frac{\partial^2 w_3}{\partial t^2} + \frac{\partial^2}{\partial x^2}\left(E_3 I_3 \frac{\partial^2 w_3}{\partial x^2}\right) - k^* w_1 + k^* w_3 \right]\delta w_3 \,\mathrm{d}x \right\} \mathrm{d}t = 0. \quad (9)$$

At this point, the arbitrariness of the virtual displacements is invoked in a judicious manner. In particular, we assume that either δw_i or its coefficient in the boundary term is zero at $x = 0$ and $x = L$, and that δw_i is entirely arbitrary over the domain $0 < x < L$, we find that equation (9) can be satisfied if and only if

$$m_1 \frac{\partial^2 w_1}{\partial t^2} + \frac{1}{4} m_2 \left(\frac{\partial^2 w_1}{\partial t^2} + \frac{\partial^2 w_3}{\partial t^2}\right) + \frac{\partial^2}{\partial x^2}\left(E_1 I_1 \frac{\partial^2 w_1}{\partial x^2}\right) + k^*(w_1 - w_3) = 0 \quad (10a)$$

and

$$\frac{1}{4} m_2 \left(\frac{\partial^2 w_1}{\partial t^2} + \frac{\partial^2 w_3}{\partial t^2}\right) + m_3 \frac{\partial^2 w_3}{\partial t^2} + \frac{\partial^2}{\partial x^2}\left(E_3 I_3 \frac{\partial^2 w_3}{\partial x^2}\right) + k^*(w_3 - w_1) = 0 \quad (10b)$$

over $0 < x < L$ and subjected to the necessary boundary conditions. The boundary conditions are that either the shear force or displacement is specified by

$$\frac{\partial}{\partial x}\left(E_i I_i \frac{\partial^2 w_i}{\partial x^2}\right) = 0 \quad \text{or} \quad w_i = 0, \quad (11)$$

at $x = 0$ or L and that either the moment or slope is defined by

$$E_i I_i \frac{\partial^2 w_i}{\partial x^2} = 0 \quad \text{or} \quad \frac{\partial w_i}{\partial x} = 0, \tag{12}$$

at $x = 0$ or L for $i = 1$ or 3 for the base beam or constraining layer, respectively.

This pair of coupled differential equations presented in equations (10a) and (10b) are very similar to the coupled set of equations presented by Douglas and Yang [6] with the exception of the additional terms for the mass of the viscoelastic core. These are especially important as the mass of the base beam and constraining layer is reduced, and the thickness of the viscoelastic core increased. Assuming homogeneous material properties for the composite beam and taking the Fourier transform of equations (10a) and (10b) gives

$$-m_1\omega^2 W_1 - \frac{1}{4}m_2\omega^2(W_1 + W_3) + E_1 I_1 \frac{\partial^4 W_1}{\partial x^4} + k^*(W_1 - W_3) = 0 \tag{13a}$$

and

$$-\frac{1}{4}m_2\omega^2(W_1 + W_3) - m_3\omega^2 W_3 + E_3 I_3 \frac{\partial^4 W_3}{\partial x^4} + k^*(W_3 - W_1) = 0, \tag{13b}$$

where $W_i(x, \omega) = FFT\{w_i(x, t)\}$.

These equations can be combined into a single eighth order differential equation with complex coefficients representing the motion of the base beam. First, we rearrange equation (13a) to solve for W_3 as a function of W_1 then we substitute that expression into equation (13b), giving

$$\frac{\partial^8 W_1}{\partial x^8} + \left[\frac{(k^* - m_1\omega^2 - \frac{1}{4}m_2\omega^2)}{E_1 I_1} + \frac{(k^* - \frac{1}{4}m_2\omega^2 - m_3\omega^2)}{E_3 I_3}\right]\frac{\partial^4 W_1}{\partial x^4} + \left[\frac{\omega^4(m_1 m_3 + \frac{1}{4}m_1 m_2 + \frac{1}{4}m_2 m_3) - k^*\omega^2(m_1 + m_2 + m_3)}{E_1 I_1 E_3 I_3}\right] W_1 = 0. \tag{14}$$

This is the differential equation governing the motion of the base beam. The solution of this equation is relatively straightforward since it is quadratic in the fourth derivative with respect to W_1. Assuming a progressive wave, the solution can be written as

$$W_1(x, \omega) = \sum_i A_i e^{\lambda_i x}, \tag{15}$$

where λ_i are the eight roots of the characteristic equation and the coefficients A_i are the constants to be determined based on the boundary conditions. Since equation (14) can be represented as a quadratic equation, it has only two distinct roots. The remaining roots are the positive and negative complex conjugates of the two distinct roots.

For cantilever beam type boundary conditions, fixed-free end conditions, the four equations of constraint for the base beam require that at the clamped end,

$$W_1|_{x=L} = 0, \quad \left.\frac{\partial W_1}{\partial x}\right|_{x=L} = 0, \tag{16}$$

and at the free end

$$\left.\frac{\partial^2 W_1}{\partial x^2}\right|_{x=0} = 0, \quad \left.\frac{\partial^3 W_1}{\partial x^3}\right|_{x=0} = \frac{P_0}{E_1 I_1}. \tag{17}$$

Here, the co-ordinate system has been chosen so that $x = 0$ occurs at the free end of the cantilever beam and $x = L$ occurs at the clamped end, as shown in Figure 4. The applied sinusoidal loading, implicit to the Fourier transform of the partial differential equations, is

accounted for in the shear boundary condition. Similarly, the shear and moment are zero at both ends of the unrestrained constraining layer which yields the following four boundary conditions:

$$\frac{\partial^2 W_3}{\partial x^2} = 0, \quad \frac{\partial^3 W_3}{\partial x^3} = 0, \quad \text{at} \quad x = 0 \quad \text{and} \quad x = L. \tag{18}$$

For a constraining layer that is restrained at an end, the boundary conditions require that the slope and displacement match the slope and displacement of the base beam at the restrained end.

The eight boundary conditions can be written in matrix form to solve for the eight unknown coefficients, $A_1 - A_8$, at each frequency of interest. Once the unknown coefficients are determined, the results can be expressed in any of the traditional frequency response formulations. In terms of the receptance the results are

$$R_1(x, \omega) = \frac{1}{P_0} \sum_i A_i e^{\lambda_i x}. \tag{19}$$

The analytical frequency response functions can be analyzed and compared with experimental results.

4. EXPERIMENTAL VALIDATION

In order to test the validity of the compressional damping model in viscoelastic beams, a series of simple experiments was conducted on an additional eleven cantilever beams. These experiments used standard modal analysis techniques to determine the first two natural frequencies and damping ratios for the beams. The experimental values were then compared with the results obtained from the compressional damping model presented in the previous section and from results calculated using the Mead and Markus model [3, 4]. A comparison with the Douglas and Yang model [6] is also discussed.

The eleven cantilever beams were all 314 mm long and 25·4 mm wide with various arrangements of viscoelastic core and constraining layer thicknesses, as summarized in Table 1. All eleven beams and constraining layers were constructed of aluminum and used EAR-C1002 viscoelastic material for the damping layer. Beams 1–9 had constraining layers that were unrestrained at both ends whereas beams 10 and 11 had constraining layers that were restrained at the clamped end of the beam. This was done by lengthening the constraining layer and arranging the beam geometry such that the layer was clamped in the fixture along with the base beam, to allow a comparison of different constraining layer boundary conditions on the overall response of the beams.

Frequency response functions were obtained from the force and displacement responses of a modal force hammer and the upper MTI Fotonic fiber optic displacement sensor shown in Figure 1, respectively. The first two natural frequencies and damping ratios were extracted from the frequency response data using standard curve-fitting procedures. Data used consisted of the experimental data, as well as the frequency response data calculated using our compressional damping model and from the Mead and Markus shear damping model. The results are presented in Tables 2 and 3. Figure 5 shows a comparison of the frequency response plots obtained experimentally and with the two analytical models for Beam 6. This plot is typical of the results obtained. Table 2 also includes data generated with the Douglas and Yang model.

The results in Table 2 show that the compressional damping model estimates the first two natural frequencies with more accuracy than the Mead and Markus model. Ten of the

TABLE 1

Cantilever beam thicknesses

Beam	Base beam thickness (mm)	Viscoelastic core thickness (mm)	Constraining layer thickness (mm)
1			1·588
2	6·350	0·381	3·175
3			6·350
4			1·588
5	6·350	3·048	3·175
6			6·350
7			1·588
8	6·350	6·350	3·175
9			6·350
10†	6·350	3·048	3·175
11†	1·588	0·381	1·588

†Constraining layer restrained at clamped end.

TABLE 2

Comparison of calculated and experimental natural frequencies

		Compressional model		Mead–Markus model		Douglas–Yang model	
Beam	Experimental frequency (Hz)	Frequency (Hz)	Error (%)	Frequency (Hz)	Error (%)	Frequency (Hz)	Error (%)
First natural frequency							
1	47·3	47·3	0·1	55·7	18	47·9	1·2
2	44·5	45·2	1·5	56·6	27	45·7	2·6
3	44·2	48·5	9·7	66·9	51	48·9	11
4	43·0	44·0	2·4	48·4	13	47·9	11
5	40·9	42·3	3·6	47·6	17	45·4	11
6	40·7	44·1	8·5	55·4	36	46·6	14
7	39·6	40·7	2·8	45·0	14	47·8	21
8	38·1	39·5	3·6	44·4	17	45·3	19
9	37·8	41·0	8·5	52·0	38	45·7	21
10	48·1	42·9	−11	70·9	47	46·0	−4·3
11	36·4	26·2	−28	53·0	46	26·6	−27
Second natural frequency							
1	329	297	−9·8	376	14	300	−8·8
2	319	284	−11	423	33	287	−10
3	350	313	−11	528	51	315	−9·9
4	293	276	−6·0	357	22	300	−2·4
5	284	266	−6·2	364	28	286	0·63
6	305	293	−4·0	419	37	309	1·3
7	270	255	−5·3	344	28	300	11
8	262	249	−5·0	344	32	285	8·9
9	286	276	−3·6	388	36	307	7·3
10	285	269	−5·9	362	27	288	1·2
11	199	164	−18	303	52	167	−16

TABLE 3

Comparison of calculated and experimental damping ratios

Beam	Experimental damping ratio	Compressional model		Mead–Markus model	
		Damping ratio	Error (%)	Damping ratio	Error (%)
First natural frequency					
1	0·0223	0·0001	−22000	0·0462	110
2	0·0267	0·0015	−1700	0·0768	190
3	0·0215	0·0151	−42	0·0914	330
4	0·0214	0·0002	−11000	0·0576	170
5	0·0226	0·0023	−880	0·0663	190
6	0·0226	0·0203	−11	0·0633	180
7	0·0229	0·0003	−7500	0·0663	190
8	0·0224	0·0028	−700	0·0702	210
9	0·0231	0·0223	−4	0·0596	160
10	0·0657	1×10^{-5}	-7×10^{5}	0·1782	170
11	0·0556	9×10^{-6}	-6×10^{5}	0·0553	−1
Second natural frequency					
1	0·0513	9×10^{-5}	−57000	0·0392	−24
2	0·0826	0·0011	−7400	0·0654	−21
3	0·1084	0·0073	−1400	0·0809	−25
4	0·0914	0·0002	−46000	0·0980	7
5	0·1055	0·0015	−6900	0·1243	18
6	0·1027	0·0074	−1300	0·1274	24
7	0·0977	0·0005	−19000	0·1205	23
8	0·0967	0·0018	−5300	0·1707	77
9	0·1070	0·0072	−1400	0·1203	12
10	0·1017	0·0001	-1×10^{5}	0·1209	19
11	0·0835	7×10^{-7}	-1×10^{7}	0·1006	20

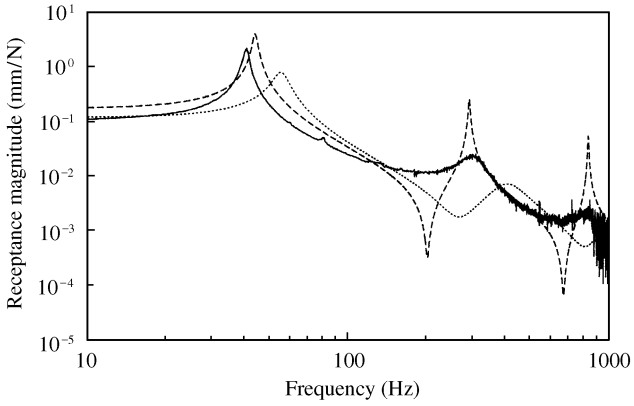

Figure 5. Experimental and analytical frequency response plots for beam 6 (——, experimental; - - - - -, compressional model; · · · · · ·, Mead and Markus model).

eleven beams are predicted within 11% and considerably more accurately in many cases, with errors as low as 0·1% and averaging 6%. In comparison, the Mead and Markus model predicts the natural frequencies with consistently higher errors; ranging from 12 to 52%.

These results show that the shear damping model couples the stiffness of the base beam and constraining layer too strongly. The first nine beams had a 314 mm × 25·4 mm × 6·35 mm base. Euler–Bernoulli beam theory gives the first two natural frequencies as 53·1 and 333 Hz for this undamped base beam. However, all the tested beams have additional mass and stiffness from the viscoelastic and constraining layers. The additional stiffness from the constraining layer causes an increase in the natural frequencies while the additional mass causes a decrease in the natural frequencies. Since all the experimental frequencies are lower than the undamped beam frequencies, it is evident that the additional mass is the dominant factor in determining the vibratory response of the beams over the added stiffness. The compressional model predicts natural frequencies that are very close to the experimental values and are all less than the undamped beam frequencies. In contrast, most frequencies predicted by the shear damping model are higher than the undamped beam frequencies, implying that the stiffness from the constraining layer has a dominant effect on the frequency response.

A comparison of the experimental and predicted damping ratios is presented in Table 3. The results indicate that the compressional model predicts damping relatively poorly while the Mead and Markus model is adequate. For the first natural frequency, the compression model was relatively accurate in three of the 11 cases and the shear model was accurate in only one out of 11 cases. In addition, the compressional model consistently under-predicted the damping of the beams. This is due to neglecting the shear damping contribution. The shear damping model, on the other hand, consistently over-predicted the damping by at least a factor of two in all but one case. This severe over-prediction of damping for the first mode could lead to significant problems in design situations. For the second natural frequency, the compressional model was a fairly poor predictor in all cases, whereas the shear damping model was accurate to within 25% in most cases. The compressional damping model was generally more accurate as the stiffness of the constraining layer increased, as seen in beams 3, 6, and 9, where the constraining layer and base beam had the same thickness. This is expected, since a stiffer constraining layer will be more likely to cause stretching in the viscoelastic core rather than the viscoelastic core causing bending in the constraining layer. Similarly, the worst errors for the compressional model are seen with beams 1, 4 and 7, where the constraining layer is thinnest. This indicates that shear damping is likely the dominant damping mechanism at the second natural frequency, whereas compressional damping at this frequency is less significant.

The difference between the last two beams and the first nine is that the constraining layer for the first nine beams is unrestrained at both ends, whereas the constraining layer on the last two beams is restrained at the clamped end. This arrangement, a change in the constraining layer boundary conditions, increased the first mode damping considerably over the beams with unrestrained constraining layers. However, the second mode damping seemed to be relatively unaffected. In addition, restraining the constraining layer had the effect of making the first natural frequency stiffness-dominated instead of mass-dominated, as in the other cases. It is interesting to note that restraining one end of the constraining layer should tend to make the beam act more according to the assumptions of the shear damping models, yet the shear damping model did an equally poor job of predicting the response of beam 10. Beam 11, on the other hand, could be considered as an ideal shear damping arrangement. It had thin, relatively stiff symmetric outer layers, a very thin viscoelastic core, and a constraining layer that was restrained at one end. The prediction of damping by the Mead and Markus model for this case was quite good for both modes, however, the natural frequency predictions were some of the poorest.

Due to their similarities, it is reasonable to compare the proposed compressional model and the model presented by Douglas and Yang [6]. As was stated previously, the primary difference between the two models is the inclusion of additional terms to account for the mass of the viscoelastic core in the present model. This addition has the effect of increasing the mass without increasing the stiffness in the analytical models. As a result, the natural frequencies calculated by the proposed model are always lower than those predicted by the Douglas and Yang model, as can be seen in Table 2. For the very thin viscoelastic cores, this amounts to a very small frequency shift, whereas for the thicker viscoelastic cores, the frequency shift is quite significant. Thus, the Douglas and Yang model predicts natural frequencies that are always too high where the frequencies predicted by the proposed model appear to correlate better with the experimental data. The only exception is beam 10, where the compression models under-predict the system stiffness. The Douglas and Yang model predicts that frequency more accurately because it underestimates both stiffness and mass.

Since the only difference between the proposed model and the Douglas and Yang model is the mass of the viscoelastic core, the damping predictions are essentially identical. For example, damping for beams 8, 9, and 10 is evaluated using the Douglas and Yang model at 0·0028, 0·0227, and $6{\cdot}3 \times 10^{-6}$ for the first mode and 0·0017, 0·0072 and 10^{-4} for the second mode, respectively. The two compression models are equally poor predictors of damping for the tested beams.

5. CONCLUSIONS

In conclusion, the experimental results presented here show that compressional vibration in a three-layer viscoelastic sandwich beam is not a narrow bandwidth phenomenon, but rather a broadband vibratory mechanism for dissipating energy in the viscoelastic core.

The compressional damping model presented here is a relatively accurate and simple method for predicting resonance frequencies of systems with constrained-layer viscoelastic damping treatments. For the arrangements tested, it is a considerably better predictor of resonance frequencies than the shear damping models currently available. While it is generally true that the main purpose of three-layer damping treatments is to add damping, an accurate model for predicting natural frequencies is very important too, given the frequency dependance of the viscoelastic material and the need to know resonance frequencies in design applications. It is expected that improved frequency and damping predictions could be obtained with the addition of shear damping terms into the model. However, any shear damping should not couple the base beam and constraining layer too strongly as this would lead to predictions of a structure that is overly stiff.

Damping predictions were quite poor for the compressional model and adequate for the shear models with only a couple of exceptions. The two exceptions were both first mode damping for beams with very stiff constraining layers. However, neglecting shear damping results in consistent damping under-prediction for the compressional model. Including shear damping as well as compressional damping should greatly improve the damping predictions. The trend seen is that the geometry of the test specimen and the vibration mode studied seem to determine the significant damping mechanisms.

REFERENCES

1. E. M. Kerwin Jr. 1959 *Journal of the Acoustical Society of America* **31**, 952–962. Damping of flexural waves by a constrained viscoelastic layer.

2. R. A. DITARANTO 1965 *Journal of Applied Mechanics* **32**, 881–886. Theory of vibratory bending for elastic and viscoelastic layered finite-length beams.
3. D. J. MEAD and S. MARKUS 1969 *Journal of Sound and Vibration* **10**, 163–175. The forced vibration of a three-layer, damped sandwich beam with arbitrary boundary conditions.
4. D. J. MEAD and S. MARKUS 1970 *Journal of Sound and Vibration* **12**, 99–112. Loss factors and resonant frequencies of encastré damped sandwich beams.
5. D. J. MEAD 1982 *Journal of Sound and Vibration* **83**, 363–377. A comparison of some equations for the flexural vibration of damped sandwich beams.
6. B. E. DOUGLAS and J. C. S. YANG 1978 *American Institute of Aeronautics and Astronautics Journal* **16**, 925–930. Transverse compressional damping in the vibratory response of elastic–viscoelastic–elastic beams.
7. B. E. DOUGLAS 1986 *Journal of Sound and Vibration* **104**, 343–347. Compressional damping in three-layer beams incorporating nearly incompressible viscoelastic cores.
8. O. SYLWAN 1987 *Journal of Sound and Vibration* **118**, 35–45. Shear and compressional damping effects of constrained layered beams.
9. B.-C. LEE and K.-J. KIM 1995 *Proceedings of the American Society of Mechanical Engineers Design Technical Conferences*, 701–708. Consideration of both extensional and shear strain of core material in modal property estimation of sandwich plates.
10. C. L. SISEMORE, A. A. SMAILI and C. M. DARVENNES 1999 *Proceedings of the American Society of Mechanical Engineers Noise Control and Acoustics Division*, 223–227. Experimental measurement of compressional damping in an elastic–viscoelastic–elastic sandwich beam.
11. C. L. SISEMORE, A. A. SMAILI and J. R. HOUGHTON 1999 *Proceedings of the Tenth World Congress of the Theory of Machines and Mechanisms*, 2140–2155. Passive damping of flexible mechanism systems: experimental and finite element investigations.